Effect of Interacting Nanoparticles on the Ordered Morphology of Block Copolymer/Nanoparticle Mixtures

MOON JEONG PARK,[1] JONGNAM PARK,[2] TAEGHWAN HYEON,[2] KOOKHEON CHAR[1]

[1]School of Chemical and Biological Engineering and NANO Systems Institute,
National Core Research Center, Seoul National University, Seoul 151-744, Korea

[2]National Creative Research Center for Oxide Nanocrystalline Materials and
School of Chemical and Biological Engineering, Seoul National University, Seoul 151-744, Korea

Received 27 May 2006; revised 10 August 2006; accepted 15 August 2006
DOI: 10.1002/polb.21011
Published online in Wiley InterScience (www.interscience.wiley.com).

ABSTRACT: We investigated the effect of hard additives, that is, magnetic nanoparticles (NPs) and metal NPs, on the ordered morphology of block copolymers by varying the NP concentration. To characterize the structural changes of a block copolymer associated with different NP loadings, small-angle X-ray scattering and transmission electron microscopy were performed. Monodisperse maghemite (γ-Fe_2O_3) NPs (7 nm in diameter) and silver (Ag) NPs (6 nm in diameter) with surfaces modified with oleic acids were synthesized, and a cylinder-forming poly(styrene-*block*-isoprene) diblock copolymer was used as a structure-directing matrix for the NPs. As the NP concentration increased, domains of NP aggregates were observed for both magnetic and metal NPs. In the case of mixtures of cylinder-forming poly(styrene-*block*-isoprene) and Ag NPs with weak particle–particle interactions, random aggregates of Ag NPs were observed, and the ordered morphology of the block copolymer lost its long-range order with an increase in the NP concentration. However, regular, latticelike aggregates obtained with γ-Fe_2O_3 NPs, because of the strong interparticle interactions, induced an intriguing morphological transformation from hexagonal cylinders to body-centered-cubic spheres via undulated cylinders, whereas the neat block copolymer did not show such a morphological transition over a wide range of temperatures. The interplay between magnetic NPs and the block copolymer was also tested with magnetic NPs of different sizes. ©2006 Wiley Periodicals, Inc. J Polym Sci Part B: Polym Phys 44: 3571–3579, 2006

Keywords: diblock copolymers; nanoparticles; phase behavior; SAXS; self-assembly; TEM

INTRODUCTION

Nanostructured organic–inorganic hybrid materials constitute one of the most promising and rapidly emerging research areas in materials chemistry, as shown by examples such as optical materials,[1,2] electromagnetic devices,[3] metal catalysts,[4] and novel structural features.[5] In particular, block copolymer/nanoparticle (NP) hybrids offer diverse scientific challenges because of their ability to microphase-separate into a wide range of ordered nanostructures; the block copolymer can assemble to form alternating layers, complex cubic structures, cylinders packed in hexagonal lattices, and spheres in body-centered lattices, and NPs can then be sequestered into one domain to form ordered hybrids.[6–8] Because of their synergistic

Correspondence to: K. Char (E-mail: khchar@plaza.snu.ac.kr)

Journal of Polymer Science: Part B: Polymer Physics, Vol. 44, 3571–3579 (2006)

interaction of individual constituents, block copolymer/NP hybrids can produce a wealth of novel structural features,[9–11] and the rational design of hybrid morphology can be based on the current understanding of the phase behavior of block copolymers and copolymer–homopolymer mixtures.[12–17]

When block copolymer/NP hybrids are prepared by the blending of presynthesized NPs with a block copolymer,[18,19] not by *in situ* reduction of metal ions within one of the block domains,[20–25] the surface of NPs can be decorated with surfactant molecules with a chemical structure similar to that of a selected block, and those NPs will diffuse into the compatible block domain. In this case, the addition of NPs can alter the characteristic dimension or sometimes even the morphology of the ordered block copolymer structure[26,27] because the miscibility of NPs with a polymer matrix (or with one of the blocks) and the resulting NP stability are crucial factors. As a result, a desirable morphology can be obtained by the control of the copolymer composition, the volume fraction of NPs, and so forth.[5,18,28]

In particular, in the case of hybrids involving ferromagnetic NPs such as iron[29] and cobalt,[30] the strong magnetic interactions among NPs can cause clustering or extensive aggregation[31,32] because block copolymers are often weakly associated with NPs. Consequently, for the microphase-separated block copolymers, the addition of strongly interacting magnetic NPs can change the characteristic dimensions or even the morphology of the ordered copolymer structures.[33] In other words, a novel change in the ordered morphology can be realized by the control of the competition between NP–NP interactions and NP–block interactions. These fascinating features of interacting magnetic NPs have recently prompted much fundamental and applied research.

Recently, we investigated the effect of a casting solvent on the phase behavior of a poly(styrene-*block*-isoprene) (PS-*b*-PI) diblock copolymer mixed with magnetic maghemite (γ-Fe_2O_3) NPs.[34] The competition of the interactions between NPs and the ordering of a block copolymer against the interactions of NP themselves leads to different hybrid morphologies. In other words, for PS-*b*-PI/γ-Fe_2O_3 NP mixtures cast with a neutral solvent for both polystyrene (PS) and polyisoprene (PI) blocks, latticelike aggregates of γ-Fe_2O_3 NPs are formed by the dominant magnetic dipole interactions, whereas the NPs are selectively incorporated into the PI domains when PI-selective hexane is used.

In this study, we re-examine the phase behavior of PS-*b*-PI/γ-Fe_2O_3 NP mixtures cast with a neutral solvent by varying the size and concentration of the magnetic NPs. The phase behavior of block copolymer/silver (Ag) NP mixtures with weak particle–particle interactions is also investigated as a reference. PS-*b*-PI can serve as a model system to investigate the subtle changes in the morphology upon the addition of NPs because PS-*b*-PI has a narrow interface between the two blocks. Moreover, we can refer to existing theoretical models of NP/block copolymer mixtures[35,36] on the basis of the strong segregation limit approximation. A hexagonal cylinder (hex) forming a PS-*b*-PI diblock copolymer was used as a structure-directing matrix. The structural information was obtained by the combination of small-angle X-ray scattering (SAXS) and transmission electron microscopy (TEM).

EXPERIMENTAL

Materials

Monodisperse γ-Fe_2O_3 NPs (7 or 14 nm in diameter) and monodisperse Ag NPs (6 nm in diameter), with both surfaces modified with oleic acids, were synthesized by the reaction of iron pentacarbonyl, silver trifluoroacetate, and oleic acid.[37] A PS-*b*-PI diblock copolymer with a PS molecular weight of 39,200 g/mol and a PI molecular weight of 12,100 g/mol was synthesized by standard anionic polymerization,[38] and the prepared sample was designated SI(39–12); it had a polydispersity index of 1.02, as verified by gel permeation chromatography. Mixtures of NPs and SI(39–12) (0/100, 1/99, 3/97, 5/95, 7/93, 10/90, and 15/85 w/w) were prepared via solution casting with toluene as a casting solvent. All the samples were annealed in a vacuum oven for 7 days at 120 °C, which was well above the glass-transition temperatures of both PS and PI.

TEM

TEM was performed on a JEOL JEM-3000F microscope. The specimens were stained by exposure to osmium tetroxide (OsO_4) vapor for 20 min. For TEM measurements, electron-transparent films with nominal thicknesses of 50–80 nm were cryomicrotomed at −90 °C with a diamond knife on a Leica Ultracut UCT and transferred to Cu grids.

SAXS

Synchrotron SAXS measurements were carried out at the 4C1 SAXS beam line at the Pohang Light Source ($\lambda = 1.54$ Å and $\Delta\lambda/\lambda = 5 \times 10^{-4}$) consisting of Si (111) double-crystal monochromators, ion chambers, and a two-dimensional position-sensitive detector with 2048 pixels × 2048 pixels. The typical beam size was smaller than 1×1 mm^2, and the sample-to-detector distance was 2.16 m. The sample temperature was controlled within ±0.2 °C with a thermostated brass block, and at least 5 min of equilibration time was allowed at a given temperature before measurement. The resulting two-dimensional scattering images were averaged azimuthally to obtain traces of the intensity versus scattering wave vector $\mathbf{q}$ [$\mathbf{q} = 4\pi\sin(\theta/2)/\lambda$, where θ is the scattering angle].

RESULTS AND DISCUSSION

To characterize the structural changes in the block copolymer associated with different NP concentrations, TEM was first performed. The stained PI phase appears dark, whereas PS is bright in the TEM micrographs. The micrographs reveal the following novel features. We can observe the clear morphological transition of hex (without NP) → undulated hex (with 5 wt % 7-nm γ-Fe_2O_3 NPs) → cubic spheres (with 10 wt % 7-nm γ-Fe_2O_3 NPs). In our case, 1 wt % of 7-nm γ-Fe_2O_3 NPs is equivalent to 0.4 vol % of γ-Fe_2O_3 NPs on the basis of the densities of γ-Fe_2O_3 NPs (2.583 g/cm^3), PS (1.05 g/cm^3), and PI (1.015 g/cm^3). With an increase in the NP concentration, the magnetic NPs clearly form strings, and this behavior confirms the previous study,[39] in which magnetic interactions between NPs favor clustering, particularly in the form of strings. For an NP concentration of 5 wt %, as shown in Figure 1(a), extensively aggregated strings can be observed, and TEM confirms the fluctuation or undulation of the ordered block copolymer perturbed by the existence of stringlike γ-Fe_2O_3 NP aggregates. For an NP concentration of 10 wt %, the magnetic NPs aggregate into self-assembled lattices, and the block copolymer morphology shows body-centered-cubic (bcc) spheres, as shown in Figure 1(b).

To better understand the morphological changes with the variation of the NP concentration, synchrotron SAXS measurements were undertaken for 7-nm γ-Fe_2O_3 NP/SI(39–12) mixtures, as shown in Figure 2. For neat SI(39–12), the $\mathbf{q}/\mathbf{q}^*$ ratios of

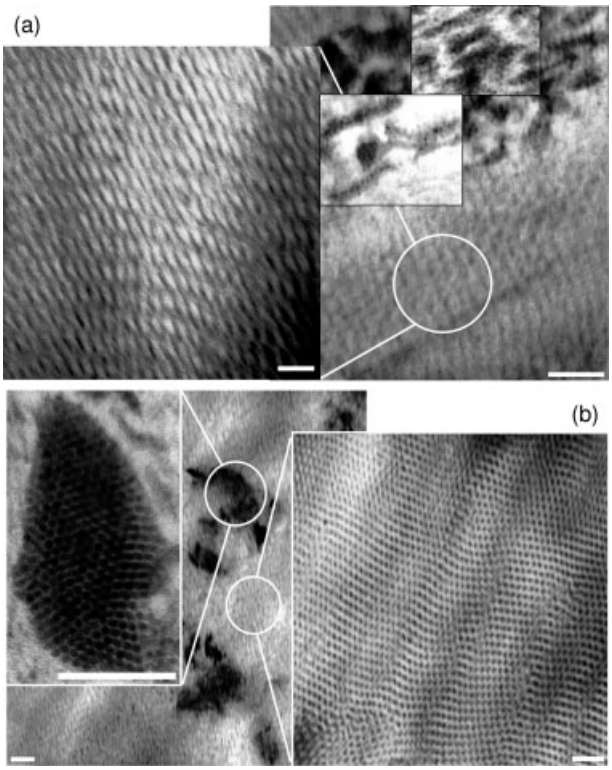

Figure 1. Cross-sectional TEM images of (a) 5/95 and (b) 10/90 (w/w) 7-nm γ-Fe_2O_3 NP/SI(39–12) mixtures stained with OsO_4. The PI domain is shown by black images, and even darker images are dispersed γ-Fe_2O_3 NPs 7 nm in diameter. TEM images of (a) undulated cylinders of SI(39–12) and (b) latticelike, magnetic NP aggregates and cubic spheres of SI(39–12) are also shown. Two additional TEM images in part a, highlighting the NP strings, were obtained by the electron beam being focused onto NPs. All the scale bars are 100 nm.

$1{:}\sqrt{3}{:}\sqrt{7}{:}\sqrt{9}$ (the lower trace in Fig. 2), where $\mathbf{q}^* = 2\pi/d_{100}$ and d_{100} is the domain spacing between hex microdomains, as indicated by inverted, open triangles, represent the hex morphology of the block copolymer. The $\sqrt{4}\mathbf{q}^*$ reflection is relatively weak because of the coincident extinction with the cylinder form factor. The scattered intensity of the first peak gradually decreases, and high-order peaks are much smeared with an increase in the NP concentration up to 5 wt %; this is in good agreement with the TEM result in Figure 1(a) showing undulated cylinders. However, the main peak intensity is again increased above the NP concentration of 5 wt %, and a well-developed bcc phase is finally obtained for 15 wt % NP, as indicated by inverted, filled triangles with $\mathbf{q}/\mathbf{q}^*$ ratios of $1{:}\sqrt{2}{:}\sqrt{3}{:}\sqrt{4}{:}\sqrt{6}{:}\sqrt{8}{:}\sqrt{9}$ (the upper trace in

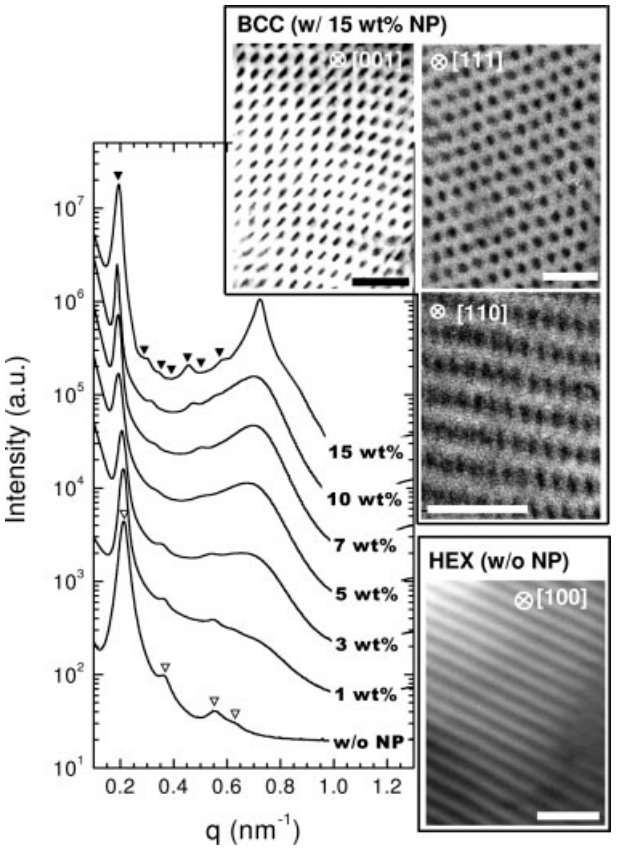

Figure 2. SAXS profiles for 7-nm γ-Fe_2O_3 NP/SI(39–12) mixtures as a function of the NP concentration. ($\triangledown$) The lower trace of neat SI(39–12) represents the hex phase with a **q** ratio of $1{:}\sqrt{3}{:}\sqrt{7}{:}\sqrt{9}$. ($\blacktriangledown$) The upper trace with 15 wt % NPs shows the well-developed bcc phase extending up to the 9th order. Definitive lattice assignments of TEM images were also obtained from neat SI(39–12) and a 15 wt % γ-Fe_2O_3 NP loading. All the scale bars are 100 nm.

Fig. 2) where $\mathbf{q}^* = 2\pi/d_{110}$, where d_{110} is the domain spacing between bcc microdomains. At the same time, the scattering intensity around $\mathbf{q} = 0.73$ nm^{-1}, originating from the NP correlation, significantly increases, signaling dominant NP aggregation. The unique morphological transformation is again confirmed with TEM in Figure 2. Without an NP loading, the TEM image clearly shows the hex morphology viewed in the [100] direction. In contrast, with the 15 wt % NP loading, the block copolymer morphology is completely transformed into the bcc structure. Three zone axes have been obtained on the basis of the feature of each TEM image, and they are all in excellent agreement with the TEM image simulation using the CaRIne Crystallography packages.[40] It should be emphasized at this point that no order–order transition has been observed for neat SI(39–12) up to 200 °C. In addition, SI(39–12) is in the vicinity of the bcc and hex phase in the block copolymer phase diagram, and this makes the morphological transition between hex and bcc rather easy if triggered by external means. In this study, the external mean should be coexisting magnetic NPs or, more specifically, extensively aggregated, latticelike NPs.

During the hex-to-bcc transition induced by coexisting magnetic NPs, we observed an interesting change in the **q*** value as a function of the NP concentration. Figure 3 shows that the **q*** value decreases abruptly for the 5 wt % NP concentration, which is the same concentration at which undulated cylinders are observed. After the formation of cubic spheres with a 10 wt % NP concentration, no considerable change in the **q*** value was observed. d_{100} is 296 Å without γ-Fe_2O_3 NPs, whereas d_{110} is 330 Å with 15 wt % γ-Fe_2O_3 NPs. As a result, the difference in the domain spacing between bcc and hex is about 11.4%, which is in good agreement with the conservation of volume, which requires the diameter of hex cylinders to be smaller than that of spherical microdomains.

The hex → bcc transformation of block copolymers is a well-known mechanism, and the existence of a metastable or even long-lived undulated hex phase during the transition has been reported.[41] However, the phenomena observed in

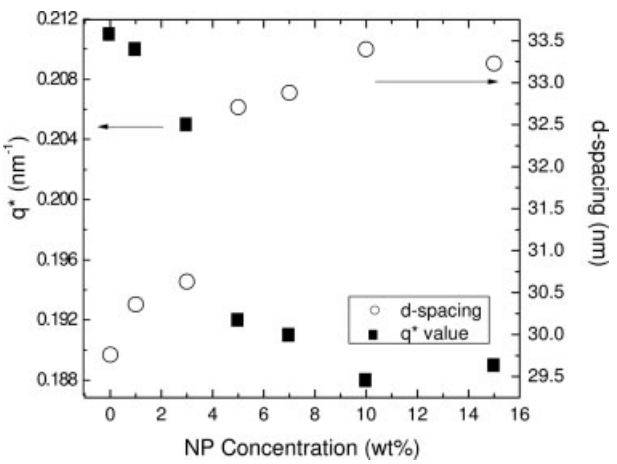

Figure 3. Changes in the **q*** and d-spacing values as functions of the NP concentration. The **q*** value decreases abruptly for the 5 wt % NP concentration because of the development of undulated cylinders. After the formation of cubic spheres above a 7 wt % NP concentration, no considerable change in the **q*** value can be observed. The d-spacing values, defined by $2\pi/\mathbf{q}^*$, are also given.

this study are quite intriguing because morphological transitions have typically been predicted when small NPs, which are much smaller than the domain size of a block copolymer, are selectively dispersed into one of the blocks.[42] In this respect, one might expect the origin of the hex-to-bcc transition to be the preferential distribution of NPs into the PS domains. However, the interfacial tensions, which are related to the surface tensions (γ_{PS} = 40.7 dyn/cm, γ_{PI} = 30.5 dyn/cm, and $\gamma_{octadecene}$ = 28.1 dyn/cm at 20 °C) and the polarity of the two contiguous phases,[43] are calculated as $\gamma_{PS/NP}$ = 7.38 dyn/cm and $\gamma_{PI/NP}$ = 0.33 dyn/cm on the basis of the harmonic mean equation.[44] This implies that the NP surfaces prefer the PI block over the PS block.

It is also worthwhile to observe that a majority of γ-Fe_2O_3 NPs are macroscopically segregated from the block copolymer domains, and as a result, the hex cylinder → cubic sphere transition is not due to the selective dispersion of γ-Fe_2O_3 NPs into one of the blocks. Figure 4 clearly confirms that the γ-Fe_2O_3 NP aggregates are macroscopically segregated from the block copolymer domains at a 10 wt % NP loading. Compared with the bright-field TEM image [Fig. 4(a)], a dark-field TEM image [Fig. 4(b)] using the (311) reflections of γ-Fe_2O_3 NPs serves as definite evidence for the segregation of NPs from block copolymer domains. To the best of our knowledge, this morphological transition of a block copolymer triggered by coexisting latticelike NP aggregates has never been reported before.

Because the new bcc structure of the block copolymer emerges through the undulated hex triggered by coexisting NPs, we can now address the following important questions: What is the role of coexisting magnetic NPs in causing such a peculiar morphological transition? Is it truly general behavior in the sense that the hex phase follows the same phase sequence (i.e., hex → bcc) upon mixing with other types of NPs? A particular emphasis is placed on the case without significant particle–particle interactions such as metal NPs. From a theoretical point of view,[35,36] both dynamic mean-field density functional theory and Monte Carlo simulations, when the particle–particle interaction is not taken into account, predict that as the NP volume fraction is increased, a two-phase coexistence, macroscopically phase-separated NP aggregates and block copolymers, emerges when the size of the NPs becomes comparable to the radius of gyration of a minority block. The formation of such phases is due to the interplay between the particle–particle excluded-volume interaction, the preferential interaction between the particles and one of the blocks, and the enthalpic and stretching interactions within the bock copolymer. However, the morphological transition between ordered structures of a block copolymer perturbed by coexisting NPs has not been reported, and a disor-

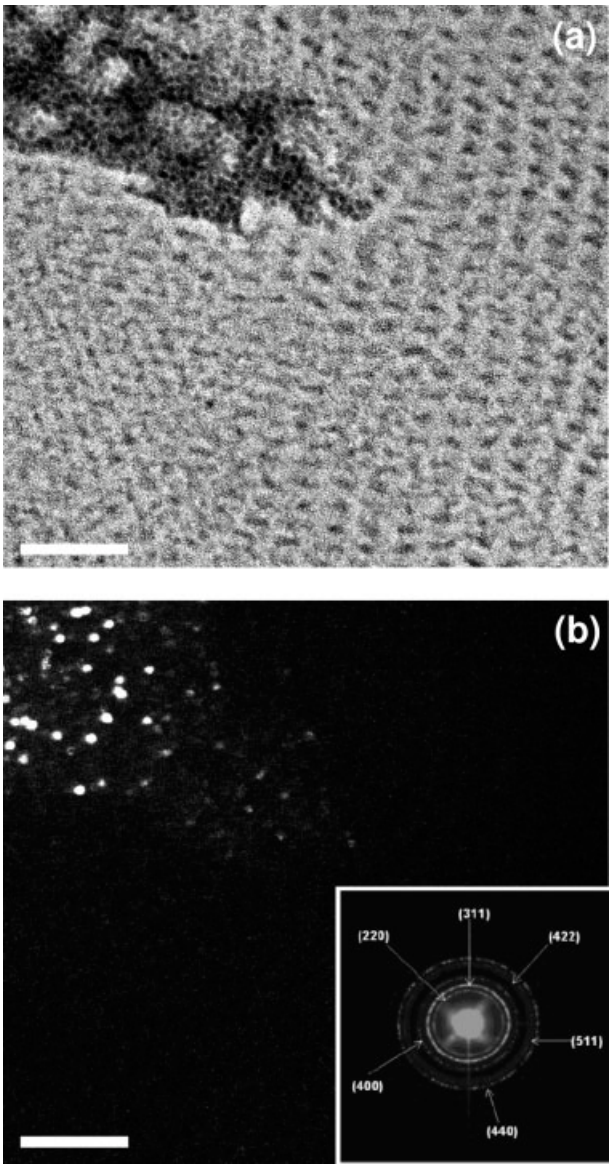

Figure 4. (a) Bright-field and (b) dark-field TEM images of a 7-nm γ-Fe_2O_3 NP/SI(39–12) (10/90 w/w) mixture. The dark-field TEM experiment is mainly intended for the detection of the (311) plane of γ-Fe_2O_3 NPs in the mixture and clearly confirms that the γ-Fe_2O_3 NP aggregates are macroscopically segregated from the block copolymer domains. All the scale bars are 100 nm.

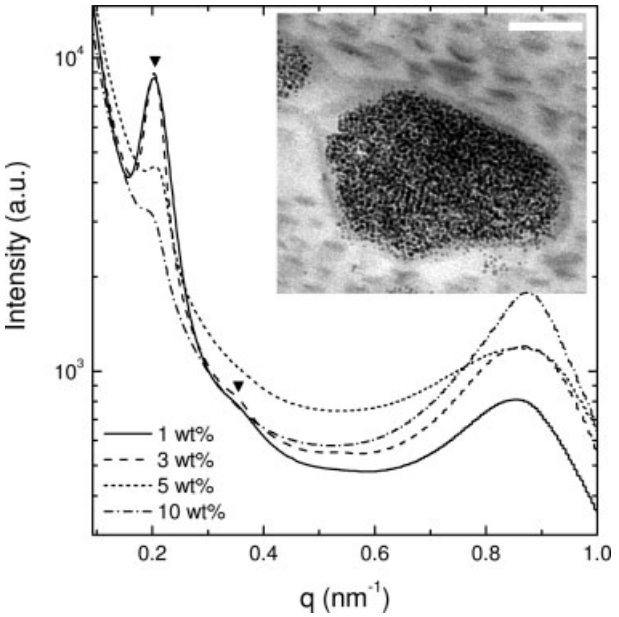

Figure 5. SAXS profiles for Ag NP/SI(39–12) mixtures with increasing NP concentration. For 1 and 3 wt % concentrations of Ag NPs, the inverted, black triangles represent the peaks with a peak ratio of 1:$\sqrt{3}$, corresponding to the hex structure, whereas the hex morphology loses its long-range order for NP concentrations above 5 wt %. The inset shows a TEM image of massively aggregated Ag NPs in SI(39–12) with a 10 wt % NP loading.

dered morphology is instead expected when the NP concentration is increased.

To investigate the effect of particle–particle interactions on the block copolymer morphology, we introduced Ag NPs 6 nm in diameter into SI(39–12). Synchrotron SAXS profiles for Ag NP/SI(39–12) mixtures with increasing NP concentration are shown in Figure 5. For 1 and 3 wt % NP concentrations, inverted, filled triangles represent the hex phase with high-order peaks of 1:$\sqrt{3}$. With an increase in the NP concentration, however, the hex morphology gradually loses its long-range order, as confirmed by the abrupt decrease in the scattered intensity of the first peak and the disappearance of high-order peaks; this is also consistent with previous theories[35,36] but is in striking contrast to the case of γ-Fe_2O_3 NPs. The scattering peaks at $\mathbf{q} = 0.87$ nm^{-1} corresponding to the NP correlation indicate that NP aggregation is also feasible with metal NPs, as already predicted by theory.[35,36] However, in contrast to γ-Fe_2O_3 NPs of a similar size, the scattering intensity of the NP correlation is not much dependent on the NP concentration, and this implies the random aggregation of Ag NPs; this is also confirmed by the TEM image of Ag NP/SI(39–12) (10/90 w/w), as shown in the inset of Figure 5. Interestingly, the TEM image shows a gray band of PI blocks 12 nm thick preferentially wetting the aggregated Ag NPs. This distinct wetting of the block copolymer plays an important role in the disordering of the block copolymer morphology as a function of the NP concentration.

We also examined the interplay between the block copolymer and magnetic NPs of different sizes. When larger magnetic NPs (i.e., 14-nm γ-Fe_2O_3 NPs instead of 7-nm NPs) are employed in the mixture, the same hex → bcc transformation can be observed even with a lower NP concentration of 3 wt %, presumably because of the enhanced magnetic interactions. Figure 6(a) shows the cross-sectional TEM images of 14-nm γ-Fe_2O_3 NP/SI(39–12) (3/97 w/w) stained with OsO_4 in different regions. The block copolymer morphology is again in good agreement with the bcc structure. Extensive hexagonal packing of self-assembled 14-nm γ-Fe_2O_3 NPs, instead of stringlike aggregates whose size measures from a few hundred nanometers to micrometers, has also been confirmed with TEM as well as SAXS.

The effect of the polydispersity of the size of NPs on the morphological transition is also examined. We deliberately synthesized polydisperse γ-Fe_2O_3 NPs with an average size of 7 nm, whereas the NP size varies from 4 to 10 nm because of the introduction of humidity during the synthesis. To our surprise, the initial hex morphology remains with an increase in the NP concentration, and the NP aggregates cannot form regular, latticelike aggregates up to a 20 wt % NP loading. Figure 6(b) shows a representative example with a 10 wt % NP loading. In this case, with an increase in the NP concentration, the number of NP aggregates 50–100 nm in size increases instead of the increased size of NP aggregates for the case with monodisperse NPs. This implies that the hex-to-bcc transition, shown with monodisperse NPs, does not occur with polydisperse NPs, and this could also serve as indirect evidence for the role of NP lattices in the morphological transformation.

Finally, we infer that the unique morphological behavior observed in this study is due to the specific particle–particle interaction leading to latticelike aggregates. For magnetic NPs, the effect of the magnetic dipole interaction is huge, and it can significantly expand the range of interparticle interactions. Thus, we expect strong magnetostatic interactions between magnetic dipole

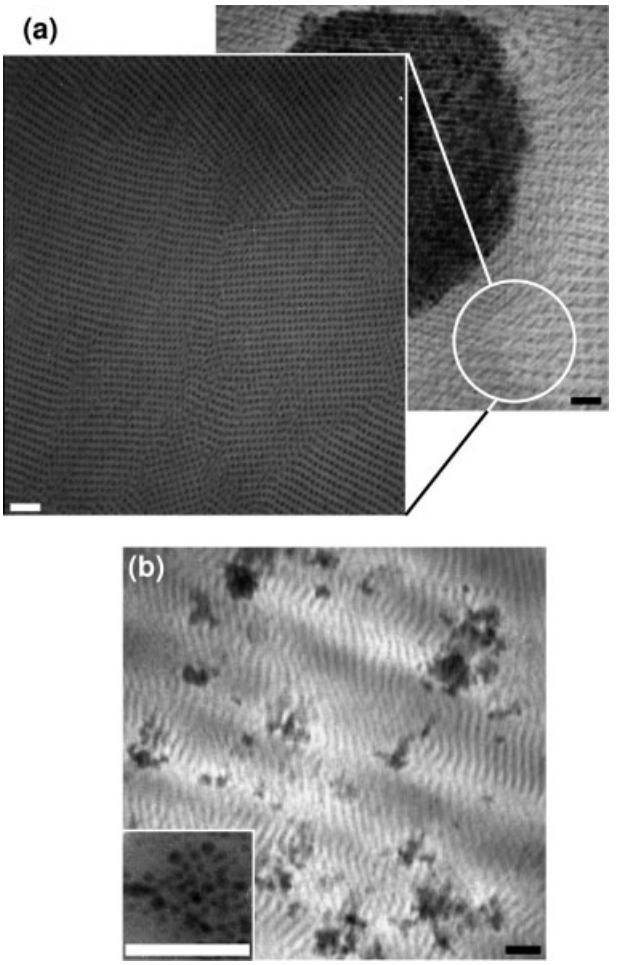

Figure 6. (a) Cross-sectional TEM images of 14-nm γ-Fe_2O_3 NP/SI(39–12) (3/97 w/w) stained with OsO_4. The bcc spheres of SI(39–12) and hexagonally packed NP aggregates are verified in separate images. (b) TEM image of polydisperse γ-Fe_2O_3 NP/SI(39–12) (10/90) indicating the hex morphology of the block copolymer. A randomly aggregated structure obtained with polydisperse γ-Fe_2O_3 NPs, which is quite different from the latticelike aggregates observed with monodisperse NPs, is also shown in the inset. All the scale bars are 100 nm.

moments as NP strings are formed,[45] and the magnetic attraction is estimated to be most dominant for 14-nm γ-Fe_2O_3 NPs coated with oleic acids.[46] In this study, different interparticle interactions are shown by different aggregation behaviors when different types of NPs are mixed with a given block copolymer. As shown in Figure 7, with a fixed NP loading of 5 wt %, the high-order peaks of 1:2:3 for 7-nm γ-Fe_2O_3 NP and $1{:}\sqrt{3}{:}\sqrt{4}{:}\sqrt{7}{:}\sqrt{9}{:}\sqrt{11}{:}\sqrt{12}\ldots$ for 14-nm γ-Fe_2O_3 NP represent the formation of strings and hexagonal lattices, respectively, whereas a single peak for Ag NP aggregates indicates randomly aggregated NPs. When latticelike γ-Fe_2O_3 NP aggregates are formed, the PI block chains preferentially diffuse into the interstitial space of NP lattices without perturbing the NP lattices, and at the same time, the NP surfaces are wetted by PI chains. We believe that this could induce packing frustration near the NP aggregates, and the ordering wave emanating from the regular, undulated surfaces of latticelike γ-Fe_2O_3 NP aggregates can cause interfacial fluctuations between PS and PI block domains. Eventually, at a higher NP loading, the ordering wave triggers the ultimate transformation from hexagonal, cylindrical domains into bcc spheres.

CONCLUSIONS

The phase behavior of a PS-*b*-PI diblock copolymer, that is, cylinder-forming SI(39–12), doped

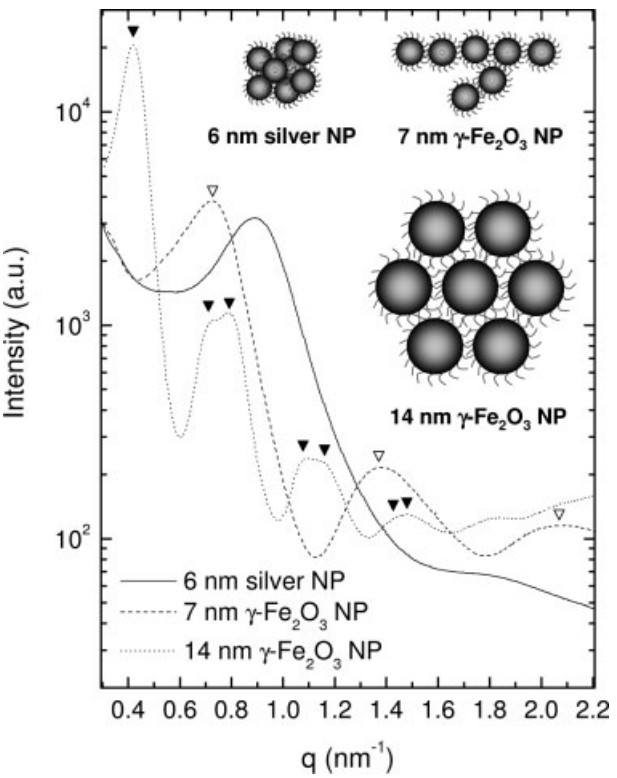

Figure 7. SAXS profiles in a high **q** range showing the NP correlation for mixtures of the block copolymer with 6-nm Ag NPs, 7-nm γ-Fe_2O_3 NPs, and 14-nm γ-Fe_2O_3 NPs at a fixed 5 wt % NP loading. The inverted, open triangles (7-nm γ-Fe_2O_3 NPs) and inverted, filled triangles (14-nm γ-Fe_2O_3 NPs) show the **q** ratios of $1{:}2{:}3$ and $1{:}\sqrt{3}{:}\sqrt{4}{:}\sqrt{7}{:}\sqrt{9}{:}\sqrt{11}{:}\sqrt{12}\ldots$, respectively.

with metal (Ag) and magnetic (γ-Fe_2O_3) NPs, has been investigated by the combination of SAXS and TEM. When the NP size is larger than the radius of gyration of a minor block, the domains of NP aggregates are observed for both magnetic and metal NPs as the NP concentration is increased. However, the block copolymer morphology significantly depends on the strength and range of particle–particle interactions. Ag NP aggregates induce a disordered micellar morphology of the block copolymer because of the preferential wetting of PI domains on Ag NP aggregates and the significant number of block copolymer chains trapped within the aggregate. In contrast, when magnetic NPs are mixed with PS-*b*-PI, segregated domains of self-assembled magnetic NPs are formed with an increase in the NP concentration, and regular, undulated surfaces of latticelike γ-Fe_2O_3 aggregates covered with low-surface-energy surfactants strongly perturb the ordering of the block copolymer. In the case of 7-nm γ-Fe_2O_3 NPs, when the NP concentration is increased above 5 wt %, fluctuations or undulations of cylindrical PI domains start to occur and eventually lead to the bcc ordered structure for higher NP concentrations. The interplay between magnetic NPs and the block copolymer has also been tested with magnetic NPs of different sizes. Notably, when the particle–particle interactions are enhanced by the size of γ-Fe_2O_3 NPs being increased from 7 to 14 nm, these peculiar morphological transitions are observed even with lower NP concentrations. This implies that the block copolymer microstructure, whether it is in hex or bcc ordered domains, can be tuned by the simple variation of the coexisting magnetic NP concentration without the alteration of the block copolymer composition. The fact that the morphology of a block copolymer can be altered by the existence of latticelike, magnetic NP aggregates, as clearly demonstrated in this study, can add more flexibility in controlling nanostructures, opening up potential for future applications.

This work was supported by the NANO Systems Institute of the National Core Research Center of the Korea Science and Engineering Foundation and by the Brain Korea 21 Program, which is endorsed by the Ministry of Education of Korea. The authors are very grateful for the use of the Pohang Light Source, which is supported by the Ministry of Science and Technology of Korea.

REFERENCES AND NOTES

1. Fendler, J. H. Nanoparticles and Nanostructured Films; Wiley-VCH: Weinheim, 1998.
2. Corbierre, M. K.; Cameron, N. S.; Sutton, M.; Mochrie, S. G. J.; Lurio, L. B.; Rühm, A.; Lennox, R. B. J Am Chem Soc 2001, 123, 10411.
3. Fink, Y.; Urbas, A. M.; Bawendi, M. G.; Joannopoulos, J. D.; Thomas, E. L. J Lightwave Technol 1999, 17, 1963.
4. Templin, M.; Franck, A.; Du Chesne, A.; Leist, H.; Zhang, Y.; Ulrich, R.; Schadler, V.; Wiesner, U. Science 1997, 278, 1795.
5. Zehner, R. W.; Lopes, W. A.; Morkved, T. L.; Jaeger, H.; Sita, L. R. Langmuir 1998, 14, 241.
6. Bockstaller, M. R.; Lapetnikov, Y.; Margel, S.; Thomas, E. L. J Am Chem Soc 2003, 125, 5276.
7. Jain, A.; Gutmann, J. S.; Garcia, C. B. W.; Zhang, Y.; Tate, M. W.; Gruner, S. M.; Wiesner, U. Macromolecules 2002, 35, 4862.
8. Ahmadi, T. S.; Wang, Z. L.; Green, T. C.; Henglein, A.; El-Sayed, M. A. Science 1996, 272, 1924.
9. Park, M.; Harrison, C.; Chaikin, P. M.; Register, R. A.; Adamson, D. H. Science 1997, 276, 1401.
10. Thurn-Albrecht, T.; Schotter, J.; Kastle, G. A.; Emley, N.; Shibauchi, T.; Krusin-Elbaum, L.; Guarini, K.; Black, C. T.; Tuominen, M. T.; Russell, T. P. Science 2000, 290, 2126.
11. Lopes, W. A.; Jaeger, H. M. Nature 2001, 414, 735.
12. Leibler, L. Macromolecules 1980, 13, 1602.
13. Bates, F. S.; Fredrickson, G. H. Annu Rev Phys Chem 1990, 41, 525.
14. Matsen, M. W.; Bates, F. S. Macromolecules 1996, 29, 1091.
15. Hamley, I. W. The Physics of Block Copolymers;Oxford: London, 1998.
16. Floudas, G.; Vazaiou, B.; Schipper, F.; Ulrich, R.; Wiesner, U.; Iatrou, H.; Hadjichristidis, N. Macromolecules 2001, 34, 2947.
17. Simon, P. F. W.; Ulrich, R.; Spiess, H. W.; Wiesner, U. Chem Mater 2001, 13, 3464.
18. Chiu, J. J.; Kim, B. J.; Kramer, E. J.; Pine, D. J. J Am Chem Soc 2005, 127, 5036.
19. Thompson, R. B.; Rasmussen, K. Ø.; Lookman, T. Nano Lett 2004, 4, 2455.
20. Morkved, T. L.; Wiltzius, P.; Jaeger, H. M.; Grier, D. G.; Witten, T. A. Appl Phys Lett 1994, 64, 422.
21. Sakai, T.; Alexandridis, P. Langmuir 2004, 20, 8426.
22. Spatz, J. P.; Roescher, A.; Möller, M. Adv Mater 1996, 8, 337.
23. Tamai, H.; Sakurai, H.; Hirota, Y.; Nishiyama, F.; Yasuda, H. J Appl Polym Sci 1996, 56, 441.
24. Saito, R.; Okamura, S.; Ishizu, K. Polymer 1993, 34, 1183.

25. Chan, Y. N. C.; Craig, G. S. W.; Schrock, R. R.; Cohen, R. E. Chem Mater 1992, 4, 885.
26. Ribbe, A. E.; Okumura, A.; Matsushige, K.; Hashimoto, T. Macromolecules 2001, 34, 8239.
27. Wang, Q.; Nealey, P. F.; de Pablo, J. J. J Chem Phys 2003, 118, 11278.
28. Hashimoto, T.; Harada, M.; Sakamoto, N. Macromolecules 1999, 32, 6867.
29. Tronc, E.; Fiorani, D.; Noguès, M.; Testa, A. M.; Lucari, F.; D'Orazio, F.; Grenèche, J. M.; Wernsdorfer, W.; Galvez, N.; Chanéac, C.; Mailly, D.; Jolivet, J. P. J Magn Magn Mater 2003, 262, 6.
30. Euliss, L. E.; Grancharov, S. G.; O'Brien, S.; Deming, T. J.; Stucky, G. D.; Murray, C. B.; Held, G. A. Nano Lett 2003, 3, 1489.
31. Smith, T. W.; Wychick, D. J Phys Chem 1980, 84, 1621.
32. Thomas, J. R. J Appl Phys 1966, 37, 2914.
33. Tadd, E. H.; Bradley, J.; Tannenbaum, R. Langmuir 2002, 18, 2378.
34. Park, M. J.; Park, J.; Hyeon, T.; Char, K. Langmuir 2006, 38, 1375.
35. Thompson, R. B.; Ginzburg, V. V.; Matsen, M. W.; Balazs, A. C. Science 2001, 292, 2469.
36. Huh, J.; Ginzburg, V. V.; Balazs, A. C. Macromolecules 2000, 33, 8085.
37. Hyeon, T.; Lee, S. S.; Park, J.; Chung, Y.; Na, H. B. J Am Chem Soc 2001, 123, 12798.
38. Hanley, K. J.; Lodge, T. P.; Huang, C.-I. Macromolecules 2000, 33, 5918.
39. Burke, N. A. D.; Stöver, H. D. H.; Dawson, F. P. Chem Mater 2002, 14, 4752.
40. Yu, K.; Wu, X.; Brinker, C. J.; Ripmeester, J. Langmuir 2003, 19, 7282.
41. Ryu, C. Y.; Lodge, T. P. Macromolecules 1999, 32, 7190.
42. Yeh, S.-W.; Wei, K.-H.; Sun, Y.-S.; Jeng, U.-S.; Liang, K. S. Macromolecules 2005, 38, 6559.
43. Brandrup, J.; Immergut, E. H.; Grulke, E. A. Polymer Handbook, 4th ed.; Wiley: New York, 1998.
44. Wu, S. Polymer Interface and Adhesion;Marcel Dekker: New York, 1982.
45. Kechrakos, D.; Trohidou, K. N. Phys B 2002, 318, 360.
46. Scholten, P. C. In Studies of Magnetic Properties of Fine Particles and Their Relevance to Materials Science; Dormann, J. L.; Fiorani, D., Eds.; Elsevier: Amsterdam, 1992.